Front. Earth Sci. 2020, 14(1): 124–139
https://doi.org/10.1007/s11707-019-0759-7

RESEARCH ARTICLE

Spatial patterns of net primary productivity and its driving forces: a multi-scale analysis in the transnational area of the Tumen River

Jianwen WANG[1], Da ZHANG (✉)[1], Ying NAN[1], Zhifeng LIU[2,3], Dekang QI[1]

1 Department of Geography, Yanbian University, Yanji 133002, China
2 Center for Human-Environment System Sustainability (CHESS), State Key Laboratory of Earth Surface Processes and Resource Ecology (ESPRE), Faculty of Geographical Science, Beijing Normal University, Beijing 100875, China
3 School of Natural Resources, Faculty of Geographical Science, Beijing Normal University, Beijing 100875, China

Abstract Analyzing the spatial patterns of net primary productivity (NPP) and its driving forces in transnational areas provides a solid basis for understanding regional ecological processes and ecosystem services. However, the spatial patterns of NPP and its driving forces have been poorly understood on multiple scales in transnational areas. In this study, the spatial patterns of NPP in the transnational area of the Tumen River (TATR) in 2016 were simulated using the Carnegie Ames Stanford Approach (CASA) model, and its driving forces were analyzed using a stepwise multiple linear regression model. We found that the total amount of NPP in the TATR in 2016 was approximately 14.53 TgC. The amount of NPP on the Chinese side (6.23 TgC) was larger than those on the other two sides, accounting for 42.88% of the total volume of the entire region. Among different land-use and land-cover (LULC) types, the amount of NPP of the broadleaf forest was the largest (11.22 TgC), while the amount of NPP of the bare land was the smallest. The NPP per unit area was about 603.21 gC/($m^2 \cdot yr$) across the entire region, while the NPP per unit area on the Chinese side was the largest, followed by the Russian side and the DPRK's side. The spatial patterns of NPP were influenced by climate, topography, soil texture, and human activities. In addition, the driving forces of the spatial patterns of NPP in the TATR had an obvious scaling effect, which was mainly caused by the spatial heterogeneity of climate, topography, soil texture, and human activities. We suggest that effective land management policies with cooperation among China, the DPRK, and Russia are needed to maintain NPP and improve environmental sustainability in the TATR.

Received September 23, 2018; accepted April 15, 2019

E-mail: zhangda@ybu.edu.cn

Keywords transnational area of the Tumen River, NPP, spatial pattern, driving force, multiple scale

1 Introduction

Net primary productivity (NPP) refers to the total amount of organic matter produced by photosynthesis per unit area in a unit of time after the deduction of autotrophic respiration (Holben, 1986; Cramer et al., 1999). NPP not only directly reflects the production capacity of natural vegetation, but also reveals the health status of terrestrial ecosystems. NPP is a widely recognized indicator of ecosystem functions and ecosystem services. On the one hand, it is an important factor in determining the carbon cycle in the terrestrial ecosystem. On the other hand, it is closely related to the supporting capacity of the earth and climate regulation capacity of the terrestrial ecosystem (Field et al., 1995; Matsushita and Tamura, 2002; Haberl et al., 2007). In recent years, NPP has attracted much attention from various researchers. The International Geosphere-Biosphere Programme (IGBP), the Global Change and Terrestrial Ecosystem (GCTE), and the Kyoto Protocol all regarded NPP as one of the key questions in the future (IGBP, 1998). Therefore, analyzing the spatial patterns of NPP and its driving forces has become one of the key issues in geography, ecology, and sustainability science (Ruimy et al., 1994; Prince and Goward, 1995; Zhang et al., 2017, 2019; Liu et al., 2019).

Transnational areas are the regions where two or more countries exist along the borderlines (Grant and Quinn, 2007). In transnational areas, the status of socio-economic development in different countries has exhibited an obvious difference owing to different policies and regulations of the different countries (Tao et al., 2017). For this

reason, the spatial patterns of NPP and its driving forces always exhibited an obvious difference in transnational areas. It is very important to analyze the spatial patterns of NPP and its driving forces on multiple scales to explore effective land management policies for different countries in the transnational areas. The transnational area of the Tumen River (TATR) is located in the core region of northeast Asia, which is considered to be an important starting point for the future Eurasian Continental Bridge (Zhang and Tang, 2010; Li and Pan, 2018). In the "National Ecological Functional Zoning" launched by the Ministry of Environmental Protection and the Chinese Academy of Sciences in 2011, the TATR has become a major component of the "Changbai Mountain Forest Ecological Function Zone" and also an important water conservation zone (Kang et al., 2017; Tao et al., 2017). In the "Belt and Road" Initiative launched by the Chinese government in 2017, this region has become an important component of the "China-Russia-DPRK-Mongolia" international channel, which is also an important starting point for the "Land Silk Road" (Zou, 2015). Therefore, it is of great theoretical and practical significance to analyze the spatial patterns of NPP and its driving forces in the TATR to improve the environmental sustainability of this region.

Recently, several studies have been conducted to analyze the spatial patterns of NPP and its driving forces in some transnational areas and TATR. For example, Barnes et al. (2015) estimated the interannual and seasonal dynamics of NPP and analyzed its driving forces in English Channel. Zhao (2011) measured the spatiotemporal patterns of NPP in the Yarlung Zangbo River basin in the China-Indian border area from 1998 to 2007 and assessed the impacts of climate change on them. Mainuddin and Kirby (2009) analyzed the differences in the NPP of cropland in the lower reaches of the Mekong River along the borderlines of Vietnam, Cambodia, Thailand, and Laos. In the TATR, Mao et al. (2012a) simulated and analyzed the NPP dynamics and its driving forces from 1982 to 2010 by using the CASA model. However, existing studies just analyzed the spatial patterns of NPP and its driving forces on one scale (i.e., on the Chinese side) in the TATR. A multi-scale analysis of the spatial patterns of NPP and its driving forces is still lacking.

In this context, the objective of this study was to analyze the spatial patterns of NPP and its driving forces in the TATR in 2016 on multiple scales. To achieve this goal, the NPP in the TATR in 2016 was quantified using the Carnegie Ames Stanford Approach (CASA) model based on remote sensing and meteorological data. Then, the total amount of NPP and NPP per unit area were calculated in the entire region and three sub-regions (i.e., the Chinese, DPRK, and Russian sides) in 2016. Finally, a stepwise multiple linear regression model was used to quantify the driving forces of the spatial patterns of NPP on these scales.

2 Study area and data

2.1 Study area

TATR mainly includes the eastern part of Jilin Province in China, north-eastern DPRK, and the Russian Far East, which is located within 128°56′–132°25′E and 41°30′–43°44′N and covers an area of approximately 24,000 km^2 (Fig. 1). The Chinese side includes 4 cities in Jilin Province: Yanji, Longjing, Tumen, and Hunchun, which covers an area of approximately 10,100 km^2 and accounts for 42.08% of the total area of the region. The DPRK's side includes 8 cities: Chongjin, Luojin, Xianfeng, Wencheng, Saibie, Hoeryong, Funing, and Ende covering an area of approximately 6800 km^2 and representing 28.34% of the total area of the region. The Russian side includes Vladivostok, Hasan, Artem, and Nadezhdinskiy and covers an area of approximately 7100 km^2, accounting for 29.58% of the total area of the entire region. The TATR has a moderate-temperate monsoon climate with an average annual precipitation of 600–700 mm and an average annual temperature of 2°C–6°C (Nan et al., 2010, 2013; Zhu et al., 2014; Kang et al., 2017; Li et al., 2018; Yang et al., 2019).

2.2 Data

The data used in this study include land-use and land-cover (LULC) data, normalized difference vegetation index (NDVI) data, meteorological data, geographical auxiliary data, soil data, population density data, and nighttime light data. The LULC data were produced through visual interpretation based on the remotely sensed images of Landsat-8 OLI downloaded from the geospatial data cloud (Table A1). Precision validation was conducted by comparing the remote sensing data with Google Earth maps. The Kappa coefficient of LULC classification was 87.5%. The data had 12 LULC classes with a spatial resolution of 30 m, including urban land, rural settlement, dry farmland, river, lake, paddy field, marsh, grassland, bare land, coniferous forest, mixed forest, and broadleaf forest.

The NDVI data were obtained from the MODerate-resolution Imaging Spectroradiometer (MODIS) vegetation index product MOD13Q1 issued by the US Level 1 and Atmosphere Archive and Distribution System (LAADS). The data had a time resolution of 16 d and a spatial resolution of 250 m. The maximum value composites (MVC) method was used for obtaining maximum NDVI in 2016 (Holben, 1986). Meteorological data were downloaded from National Centers for Environmental Prediction/National Center for Atmospheric Research (NCEP/NCAR). The GIS auxiliary data including the national and provincial administrative boundary of China was obtained from the National Administration of

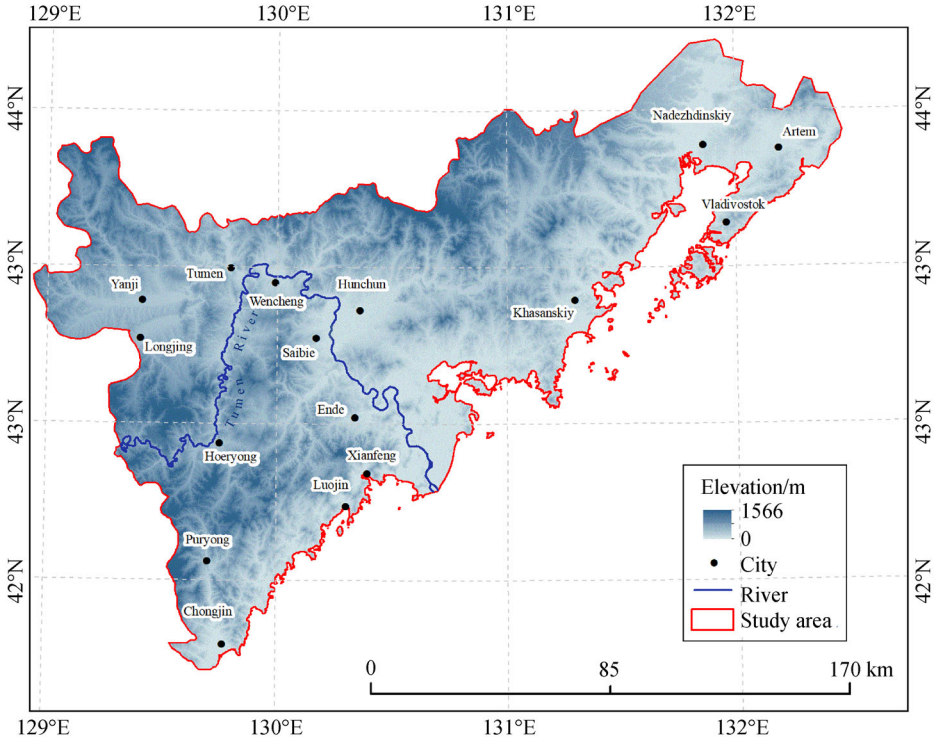

Fig. 1 The transnational area of Tumen River (TATR).

Surveying, Mapping, and Geoinformation of China. The national administrative boundaries of the DPRK and Russia were obtained from the Global Administrative Boundaries Dataset. The Shuttle Radar Topography Mission (SRTM) digital elevation model (DEM) data with a spatial resolution of 90 m were obtained from NASA and the National Mapping Agency (NMA) of the Department of Defense. The soil data were acquired from the World Soil Database. The population data were obtained from the History Database of the Global Environment (HYDE). The nighttime light data were received from the United States National Oceanic and Atmospheric Administration. All the data were resampled to a spatial resolution of 250 m.

3 Methods

3.1 Calculating NPP in the TATR in 2016

The NPP in the TATR in 2016 was estimated using the improved CASA model according to Zhu et al. (2007) and He et al. (2017). The CASA model used in this study was a satellite-based photosynthetic utilization model to calculate NPP. This model can provide a relatively effective approach to rapidly and accurately simulate the spatio-temporal pattern of NPP on a regional scale and has been widely used to evaluate NPP in many areas in China. In this model, NPP was estimated using photosynthetically active radiation and light energy efficiency which were calculated using LULC data, meteorological data, and NDVI data. Therefore, we input LULC, temperature, precipitation, NDVI, and other types of data into the CASA model to calculate NPP in the TATR. The estimated NPP can be determined by the two variables photosynthetically active radiation (APAR) and light energy efficiency (ε) absorbed by the vegetation. The NPP of cell "x" at time "t" can be calculated as follows (Eq. (1)):

$$\mathrm{NPP}(x,\ t) = \mathrm{APAR}(x,\ t) \times \varepsilon(x,\ t), \qquad (1)$$

where APAR (x, t) represents the photosynthetically active radiation absorbed by pixel "x" in month "t". $\varepsilon(x,\ t)$ represents the actual light energy efficiency rate of pixel "x" in month "t". The APAR depends on the total solar radiation and the proportion of photosynthetically active radiation absorbed by the vegetation, which is calculated as follows (Eq. (2)):

$$\mathrm{APAR}(x,\ t) = \mathrm{SOL}(x,\ t) \times \mathrm{FPAR}(x,\ t) \times 0.5, \qquad (2)$$

where SOL (x, t) represents the total solar radiation of the pixel "x" in month "t". APAR (x, t) represents the proportion of photosynthetically active solar radiation (PAR) absorbed by the vegetation. The constant of 0.5 indicates the proportion of total solar radiation (0.4–0.7) available for vegetation. There is a good linear relationship between FPAR, NDVI, and SR (Los et al., 1994). Therefore, FPAR can be estimated based on the NDVI data obtained from the MOD13Q1 product and LULC data.

According to Potter et al. (1993), the conversion rate of light energy affected by temperature and moisture refers to the efficiency of conversion of photosynthetically active radiation (PAR) absorbed by the vegetation into organic carbon, which can be calculated as follows (Eq. (3)):

$$\varepsilon(x,t) = T_{\varepsilon 1(x,t)} \times T_{\varepsilon 2(x,t)} \times W_{\varepsilon(x,t)} \times \varepsilon_{\max}, \quad (3)$$

where $T_{\varepsilon 1(x,t)}$ and $T_{\varepsilon 2(x,t)}$ indicate the impacts of temperature on the conversion rate of light energy. $W_{\varepsilon(x,t)}$ represents the effect of moisture conditions on the conversion rate of light energy which were gotten from precipitation. $\varepsilon_{\max}$ is a biome-specific light use efficiency factor that is estimated from daily meteorological conditions and shows significant differences among different LULC. $\varepsilon_{\max}$ means the maximal light use efficiency of the specific type of vegetation under ideal conditions (minimum temperature and vapor pressure deficit). The $\varepsilon_{\max}$ used in this study was obtained from Zhu et al. (2006) and Running et al. (2000) (Table A2).

3.2 Quantifying the spatial pattern of NPP

In this study, the total amount of NPP, the NPP of each LULC type, and the NPP of the four seasons were quantified based on the calculation of the CASA model. First, the total amount of NPP was quantified using the boundary data. Then, the mean NPP of different LULC types was extracted based on the LULC data in 2016, and the total amount of NPP of each LULC type was calculated based on the area of each LULC type. Finally, the mean NPP of the four seasons was calculated from the calculations of the CASA model using (Eq. (4)):

$$\overline{\mathrm{NPP}} = \frac{\sum_{i=1}^{n} \mathrm{NPP}_i}{n}, \quad (4)$$

where $\overline{\mathrm{NPP}}$ indicates the mean NPP of a season, n represents the number of months, and NPP_i means the NPP value of pixel i. In addition, the total amount of NPP and the mean NPP of each LULC type were quantified and compared on the two scales, so that the extent of our analysis covered the entire region and the three sides of China, DPRK, and Russia.

3.3 Analyzing the driving forces of spatial pattern of NPP

In this study, the driving forces of spatial pattern of NPP were analyzed. We first selected several key driving forces, then used a stepwise multiple linear regression model to analyze them after Gao (2000) and Hao et al. (2017). This method is full of simplicity, intuition, and convenience. The equation of stepwise multiple linear regression can be expressed as follows (Eq. (5)):

$$Y = \beta_0 + \beta_1 X_1 + \beta_2 X_2 + \ldots + \beta_P X_P + e, \quad (5)$$

where Y and X represent the dependent and independent variables, respectively, X_1, X_2, …, X_P represent the respective independent variable, and β_1, β_2, ..., β_P represent the partial regression coefficients indicating that when X increases or decreases by one unit, Y will increase or decrease by β units. To make the partial regression coefficients comparable, all the independent and dependent variables were normalized. The obtained regression equation is then called the standard regression equation and the regression coefficient is called the standard regression coefficient. The standard regression equation can be expressed as follows (Eq. (6)):

$$Z_Y = \beta_1 Z_{X1} + \beta_2 Z_{X2} + \ldots + \beta_P Z_{XP}, \quad (6)$$

where Z_Y refers to the normalized dependent variable and Z_{X1}, Z_{X2}, $...Z_{XP}$ represent the normalized independent variables. The absolute value of the regression coefficient indicates the degree of importance of the independent variable to the dependent variable. When the absolute value is greater, the effect will be larger (Zhan et al., 2013; Hao et al., 2017).

Due to the small areas of river, lake, swamp, and bare land, the NPP of these LULC types were not considered when analyzing the driving forces of the spatial patterns of NPP in the TATR in 2016. The driving forces of the spatial patterns of the NPP of broadleaf forest, mixed forest, coniferous forest, grassland, dry farmland, paddy field, urban land, and rural settlement were analyzed. According to several previous studies, temperature, precipitation, altitude, slope, aspect, silt, sand and clay content, distance to the coastline, distance to the nearest road, population, and night light density were strongly relevant to the spatial patterns of NPP in the TATR (Garcia-Aguirre et al., 2007; Jian, 2010; Chen et al., 2014; Sun et al., 2015; Chen et al., 2016). Specifically temperature and precipitation are regarded as important driving forces influencing the spatial pattern of NPP. When the temperature rises or the precipitation increases, the activity of enzymes in photosynthesis increases, which in turn influences the spatial pattern of NPP (Tao et al., 2003). Altitude, slope, aspect, and distance to the coastline are all important natural driving forces influencing hydrothermal distribution, which will result in differences of the spatial pattern of NPP (Li et al., 2014). In addition, distance to the nearest road, population, and night light density are all anthropogenic driving forces representing human activities, including increase in artificial buildings and socioeconomic development (Imhoff et al., 2004; Jiang, 2016; Liu et al., 2016). These anthropogenic driving forces will have a significant influence on the spatial pattern of NPP.

To analyze the driving forces of the spatial patterns of NPP, random points on the three sides of China, DPRK, and Russia were selected according to the proportion of different LULC types. Then, the value of the driving force on each random point was extracted based on spatial

analysis tools from ArcGIS. Finally, the normalized value of the random points and the values of NPP were entered into the SPSS software and the stepwise multiple linear regression model was used to quantify the major driving forces that influenced the spatial patterns of the NPP in the TATR. In this study, we used VIF (Variation Inflation Factor) to verify the effectiveness of the multiple linear regression model. According to Huang et al. (2015) and You and Yan (2017), VIF⩽3 represents that there was a multilinear relationship between explanatory variables; irrelevant variables were all removed from the input data. In this paper, we used this value (i.e., VIF⩽3) to ensure that no multilinear relationship existed and all irrelevant variables were removed (Zhang and Dong, 2007). Finally, we obtained the optimal regression equation based on VIF.

4 Results

4.1 The spatial pattern of NPP in the TATR in 2016

In 2016, the total amount of NPP in the TATR was 14.53 TgC, and the mean NPP was about 603.21 gC/(m^2·yr). The NPP was greater in the northern and eastern regions than in the central, western, and south-east regions (Fig. 2). In the northern and eastern areas of this region, the mean NPP exceeded 600 gC/(m^2·yr). Meanwhile, in the central, western, and south-eastern regions, the NPP were relatively low.

Among all the LULC types, the total amount of NPP of the broadleaf forest in the TATR was the largest, followed by the dry farmland. Bare land was the lowest. The total amount of NPP of broadleaf forest was 11.22 TgC, accounting for 77.21% of the total amount across the entire region (Table 1, Fig. 3). The amount of NPP of coniferous and mixed forest was 0.29 TgC and 0.40 TgC, respectively, which accounted for 1.99% and 2.75% of the total NPP across the entire region. The total amount of NPP in the dry farmland was 1.46 TgC, which representing 10.05% of the total NPP in the TATR. The total amount of NPP of bare land was the least, which was less than 0.01% of the total NPP across the whole region.

In the TATR in 2016, the mean value of NPP was approximately 603.21 gC/(m^2·yr) (Table 2). Among all the LULC types, the mean NPP of broadleaf forest was the largest, followed by grassland, and the mean NPP of lake was the smallest. In 2016, the mean NPP of broadleaf forest was 697.91 gC/(m^2·yr). The mean NPP of grassland was about 500.14 gC/(m^2·yr), which was lower than the average value of the entire region. In addition, the mean NPP of dry farmland, rural settlements, marsh, and paddy field all exceeded 300 gC/(m^2·yr). The average NPP of urban land was about 192.88 gC/(m^2·yr). The average NPP of the lake was the smallest at 144.06 gC/(m^2·yr).

Among the four seasons, the mean NPP in summer was the largest, followed by spring, autumn and then winter (Table 3). In summer, the mean NPP of the LULC types ranged from 25 to 130 gC/m^2. The mean NPP of broadleaf forest was the largest, i.e., 127.27 gC/m^2, while the mean NPP of the lake was the smallest, i.e., 29.72 gC/m^2. The

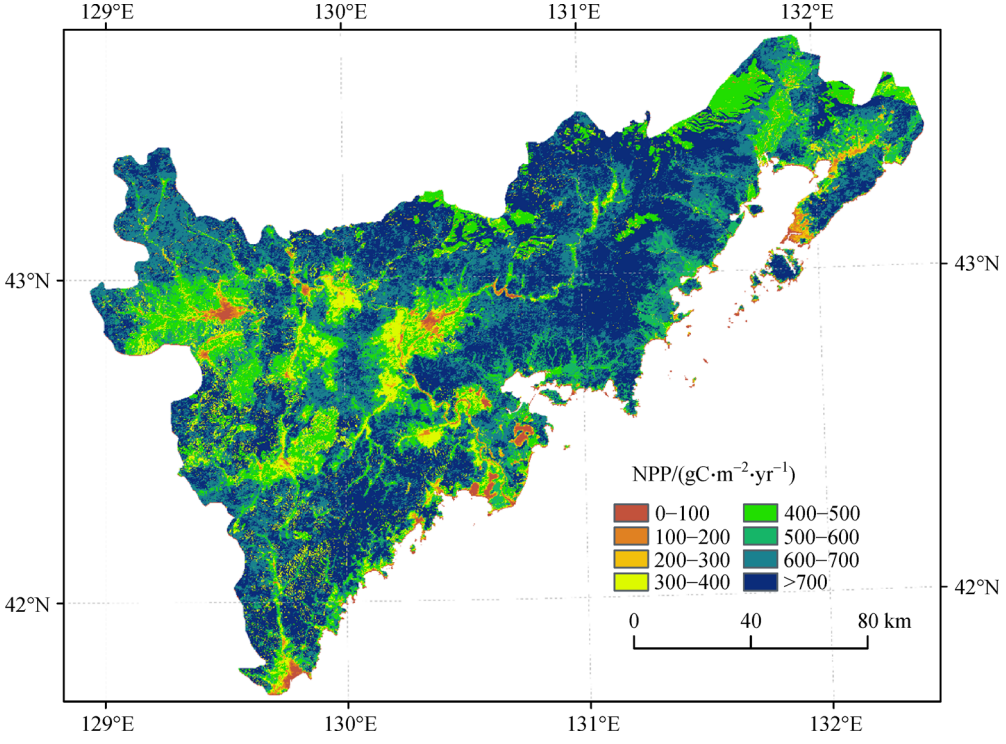

Fig. 2 The spatial pattern of NPP in the TATR in 2016.

Table 1 Total amount of NPP (TgC/yr^{-1}) of different LULC in the TATR in 2016

LULC	TATR	The Chinese side	The DPRK's side	The Russian side
Broadleaf forest	11.22	5.02	2.92	3.28
Dry farmland	1.46	0.55	0.70	0.21
Grassland	0.59	0.12	0.10	0.37
Mixed forest	0.40	0.18	0.01	0.21
Coniferous forest	0.29	0.14	0.15	0.00
Rural settlements	0.19	0.06	0.02	0.11
Paddy field	0.15	0.08	0.07	0.00
Marsh	0.08	0.01	0.01	0.06
Urban land	0.07	0.03	0.01	0.03
River	0.06	0.03	0.01	0.02
Lake	0.02	0.01	0.00	0.01
Bare land	0.00	0.00	0.00	0.00
Total amount	14.53	6.23	4.00	4.30
Percentage	100%	42.88%	27.53%	29.59%

Note: 0.00 represents the total amount of NPP is less than 0.01 TgC.

spring mean NPP ranged from 5 to 60 gC/m^2. The springtime mean NPPs of broadleaf forest, dry farmland, and mixed forest were 57.33 gC/m^2, 41.26 gC/m^2, and 35.53 gC/m^2, respectively. In autumn, the mean NPP ranged from 5 to 50 gC/m^2. In addition, the mean NPP in winter was only 2.84 gC/m^2.

4.2 The spatial pattern of NPP in the three sub-regions in 2016

In 2016, the total amount of NPP on the Chinese side was the largest, followed by the Russian and DPRK's sides. The total NPP on the Chinese side was 6.23 TgC, accounting for 42.88% of the total NPP across the whole region (Table 1, Fig. 3). Among all the LULC types, the total amount of NPP of broadleaf forest was the largest at 5.02 TgC, representing 80.58% of the total NPP on the Chinese side. Meanwhile, the total amount of NPP on the Russian side was 4.30 TgC, accounting for 29.59% of the total volume across the whole TATR. On this side, the total NPP of broadleaf forest was approximately 3.28 TgC, accounting for more than 70% of the total NPP in this area. On the DPRK side, the total NPP was only 4.00 TgC, accounting for 27.53% of the total NPP across the whole TATR.

In 2016, the average NPP on the Chinese side was the largest, followed by the Russian and the DPRK sides. The average NPP on the Chinese side was approximately 613.59 $gC/(m^2 \cdot yr)$ (Table 2). Among all the LULC types, the mean NPP of broadleaf forest was about 701.55 $gC/(m^2 \cdot yr)$, which was larger than the other LULC types. The average NPP on the Russian side was 609.06 $gC/(m^2 \cdot yr)$. Among all the LULC types, the mean NPP of broadleaf forest and grassland was 694.21 $gC/(m^2 \cdot yr)$ and 503.69 $gC/(m^2 \cdot yr)$, respectively. In addition, the mean NPP on the DPRK side was about 583.88 $gC/(m^2 \cdot yr)$. The mean NPP of broadleaf forest on the DPRK side was about 698.55 $gC/(m^2 \cdot yr)$.

4.3 The driving forces of spatial pattern of NPP in the TATR in 2016

In 2016, the spatial patterns of NPP were mainly affected by climate, topography, soil texture, and human activities in the TATR (Table A3). For broadleaf forest, the spatial pattern of NPP was mainly influenced by precipitation, altitude, and soil content. Among these driving forces, the clay content had the largest influence, and the standard partial regression coefficient was about 0.39. The irrelevant variables included temperature and aspect (Table A3). For dry farmland, the spatial pattern of NPP was positively driven by temperature, altitude, slope, silt content, and sand content. Among these driving forces, the effect of temperature was the strongest, and the standard partial regression coefficient was 0.36. In addition, the spatial pattern of NPP of dry farmland was also negatively influenced by the distance to the coastline and precipitation. The irrelevant variables included aspect and light intensity (Table A3). For urban land, the spatial pattern of NPP was mainly influenced by temperature and light intensity, and the standard partial regression coefficient of temperature was 0.54. Meanwhile, the spatial pattern of NPP of urban land was also positively affected by slope and negatively affected by population density and light intensity. All the rest of the variables were irrelevant (Table A3).

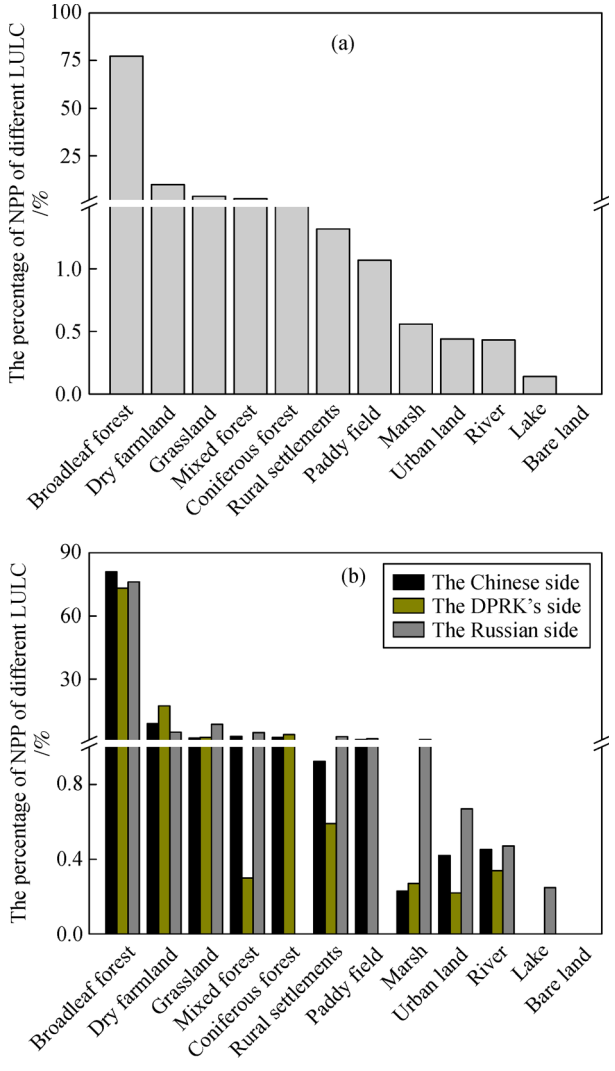

Fig. 3 The percentage of NPP of different LULC. (a) The percentage of NPP of different LULC in the TATR; (b) the percentage of NPP of different LULC in the Chinese, the DPRK's, and Russian sides.

4.4 The driving forces of spatial pattern of NPP in the three sub-regions in 2016

On the Chinese side, the spatial pattern of NPP of broadleaf forest was positively affected by altitude and soil sand content, and the standard partial regression coefficients were 0.14 and 0.17, respectively (Table A4). Meanwhile, there was a negative correlation between the spatial pattern of NPP of broadleaf forest with the distance to coastline and light intensity. Among these driving forces, distance to coastline was the most important driving force, with a standard partial regression coefficient of −0.22. The irrelevant variables included temperature, precipitation, and aspect (Table A4). The spatial pattern of NPP of dry farmland was positively influenced by slope, altitude, sand content, and distance to the nearest road, and their standard partial regression coefficients were 0.32, 0.18, 0.21, and 0.15, respectively. Meanwhile, the distance to coastline and the light intensity caused negative impacts on the spatial pattern of NPP of dry farmland, and their standard partial regression coefficients were −0.24 and −0.11, respectively. The irrelevant variables included temperature, precipitation, aspect, soil silt content, soil clay content, and population (Table A4). Finally, the main driving forces of the spatial pattern of NPP of urban land were slope, distance to the nearest road, and light intensity, with the standard partial regression coefficients of 0.20, 0.16, and −0.38, respectively. All the other variables were irrelevant. (Table A4).

On the DPRK side, the spatial pattern of NPP of broadleaf forest was mainly affected by altitude, precipitation, distance to coastline, and clay content (Table A5). The soil clay content was the most important driving force for the spatial pattern of NPP of broadleaf forest, with a standard partial regression coefficient of 0.27. Meanwhile, the spatial pattern of NPP of dry farmland was mainly influenced by altitude, slope, clay content, distance to the coastline, and light intensity, and their standard partial regression coefficients of these driving forces were 0.32, 0.31, 0.12, −0.32 and −0.1, respectively. Temperature, precipitation, soil silt content, and soil sand content were irrelevant variables (Table A5). In addition, the spatial pattern of NPP of urban land was significantly correlated with slope and light intensity.

On the Russian side, the spatial pattern of NPP of broadleaf forest was significantly correlated with precipitation, altitude, silt, and sand clay content (Table A6). The soil clay content was the most important driving force for the spatial pattern of NPP of broadleaf forest, with a standard partial regression coefficient of 0.53. The irrelevant variables included temperature, aspect, and population (Table A6). Meanwhile, the spatial pattern of NPP of dry farmland was mainly affected by slope, with a standard partial regression coefficient of 0.12. The spatial pattern of NPP of urban land was significantly influenced by precipitation, altitude, population, and light intensity. Among these four driving forces, the light intensity caused the largest impact with a standard partial regression coefficient of −0.50. On the other hand, the irrelevant variables included temperature, slope, aspect, soil sand content, soil clay content, distance to coastline, and distance to the nearest road (Table A6).

5 Discussion

5.1 Validation of results of the CASA model

Due to the uncertainties during the calculation process of NPP, it is necessary to verify the accuracy of the calculation results. The NPP verification method mainly includes direct and indirect verification (Chen et al., 2014).

Table 2 Annual mean NPP ($gC/(m^2 \cdot yr)$) of different LULC in the TATR in 2016

LULC	TATR	The Chinese side	The DPRK's side	The Russian side
Broadleaf forest	697.91	701.55	698.55	694.21
Grassland	500.14	503.09	489.87	503.69
Dry farmland	446.37	443.56	437.34	488.70
Mixed forest	413.68	412.18	393.25	417.48
Rural settlements	403.70	374.10	300.78	457.06
Paddy field	398.73	408.24	385.06	453.87
Coniferous forest	377.04	373.01	380.60	398.59
Marsh	372.50	353.17	311.52	396.99
Bare land	265.58	268.83	351.45	259.15
River	242.53	239.81	222.52	261.94
Urban land	192.88	176.68	135.22	245.05
Lake	144.06	163.88	95.41	166.40
Mean value	603.21	613.59	583.88	609.06

Table 3 Seasonal mean NPP (gC/m^2) of different LULC in the TATR in 2016

LULC	Spring	Summer	Autumn	Winter
Broadleaf forest	57.33	127.27	44.72	3.31
Dry farmland	41.26	90.68	33.11	1.66
Mixed forest	35.53	71.59	26.03	4.73
Coniferous forest	32.07	65.90	23.95	3.76
Grassland	28.78	89.97	28.60	1.44
Marsh	28.41	70.72	23.78	1.25
Rural settlements	24.18	85.38	24.43	0.59
Bare land	20.46	50.94	16.46	0.66
Paddy field	18.46	87.62	25.84	0.99
River	16.70	49.47	14.12	0.55
Urban land	10.33	41.94	11.72	0.30
lake	8.58	29.72	9.56	0.16
Mean value	48.00	111.61	38.62	2.84

Direct verification refers to comparing the NPP calculation result with the field survey data. Indirect verification refers to comparing the NPP calculation result with the NPP calculated using other methods or models. In this study, due to the lack of field survey data from China, DPRK, and Russia, the second method was used to compare the NPP calculation result with the MOD17A3 data and results of existent researches.

In this study, we first extracted NPP values from these two products. Then we compared these two kinds of NPP values. The results showed that there was a relatively good correlation relationship between these values ($R = 0.453$, $P < 0.001$, $n = 200$) (Fig. 4). The correlative coefficient was a bit small which may be the result of the disparity of the resolution of the CASA model simulation result and the MOD17A3 data, as well as the comparatively small area of the TATR. Meanwhile, other research indicated that the relatively low R coefficient might result from the difference of various study areas and the resolution of different spatial data (Zhang, 2016). In addition, to further verify the validity of the NPP calculation results, we compared our calculation results with some other products from several previous studies conducted in China and the DPRK (Table 4). The results showed that the NPP values in this study were similar with these products, which indicated that the NPP calculation results in this study could reliably reflect the real NPP in this region.

5.2 The driving forces of the spatial pattern of NPP had an obvious scaling effect in the TATR

According to Wu (2004) and Ma et al. (2018), scaling usually refers to the translation of information across spatial and temporal scales or organizational levels, which

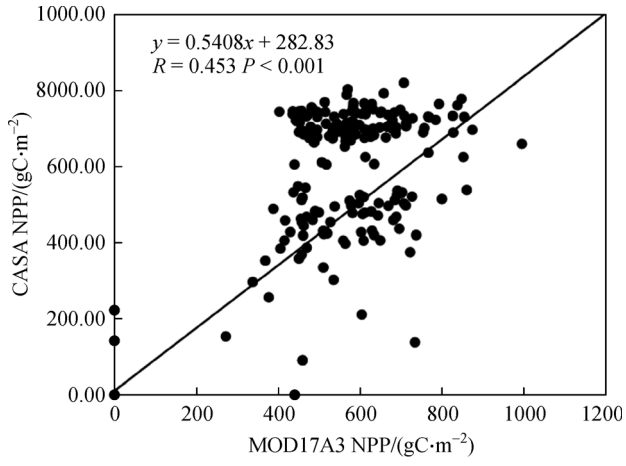

Fig. 4 Comparison of NPP between CASA and MOD17A3.

frequently involves changing grain size, extent, or both. In this study, we analyzed the driving forces of spatial pattern of NPP on two scales or in four regions, i.e., the entire TATR and the three sub-regions of China, the DPRK, and Russia. First, in the transnational area, it was essential to analyze the driving forces of the spatial pattern of NPP in different sub-regions due to the significant differences in government policies and socio-economy among different countries. Second, it would be helpful to provide effective references for environment protection and land planning for different countries. In 2016, the driving forces of spatial pattern of NPP had an obvious scaling effect in the TATR, which meant that the driving forces of spatial pattern of NPP at different scales were different (Figs. 5 and 6). Across the whole region, the spatial pattern of NPP of broadleaf forest was positively correlated with the silt content. In contrast, on the Chinese side, the spatial pattern of NPP of broadleaf forest was negatively correlated with the content of soil silt. On the Russian side, there was a positive correlation between the spatial pattern of NPP of broadleaf forest and soil silt content. In addition, there was positive significant relationship between the spatial pattern of NPP of dry farmland and temperature. However, on the sides of China, DPRK, and Russia, there was no significant correlation between the spatial pattern of NPP of dry farmland and temperature.

The differences among climate, topography, soil texture, and human activities were the main causes for the scaling effects of the driving forces of the spatial patterns of NPP (Fig. 7). The highest temperature on the Russian side was 5.38°C, and the lowest one was on the Chinese side: 4.86°C. From the perspective of precipitation, the annual precipitation on the DPRK side was the largest, followed by Russia, and the annual precipitation on the Chinese side was the smallest. From the perspective of topography, the altitude on the Chinese side was the highest, and the slope on the DPRK side was the largest. From the perspective of soil texture, the silt content on the Chinese side was the highest, the sand content on the DPRK side was the highest, and the clay content on the Russian side was the highest. Furthermore, the population density on the DPRK side was larger than those on the Chinese and Russian sides. The urban population was the highest on the Chinese side and the lowest on the DPRK side. Meanwhile, the rural population on the DPRK side was the largest. Finally, the night light intensity was the highest on the Russian side and the lowest on the DPRK side.

5.3 Implications of the spatial pattern of NPP and its driving forces for regional sustainable development in the TATR

At present, China, the DPRK, and Russia have developed a series of policies and regulations to protect the valuable land resources to maintain and improve the NPP in the TATR. China has published the “Changbai Mountain National Nature Reserve Management Regulations in Jilin Province”

Table 4 Comparison of NPP values (gC/(m^2·yr)) in this study with some other products from previous studies

LULC	This Study	Zhu et al. (2007)	Zhang and Zhou (2008)	Zhu et al. (2010)	Mao et al. (2012b)	Chen et al. (2014)	Jiang (2016)
Broadleaf forest	697.91	805.33	-	667.00	-	480.52	553.63
Mixed forest	413.68	-	572.6	615.00	-	330.3	424.14
Coniferous forest	377.04	379.62	-	564.00	-	292.02	365.94
Grassland	500.14	507.4	312.5	432.00	-	256.86	324.36
Dry farmland	446.37	426.5	309.1–331.4	503.00	400–600	282.18	410.93
Paddy field	398.73						368.75
Marsh	372.50	556.1	432.9	-	-	-	-
Urban land	192.88	347.1		-	-	211.37	-
Rural settlements	403.70	-	-	-	-	211.37	-
River	242.53	-	-	-	-	160.46	-
Lake	144.06	236.8	-	-	-	160.46	-
Mean NPP	603.21	323.8	-	426	-	-	439.42

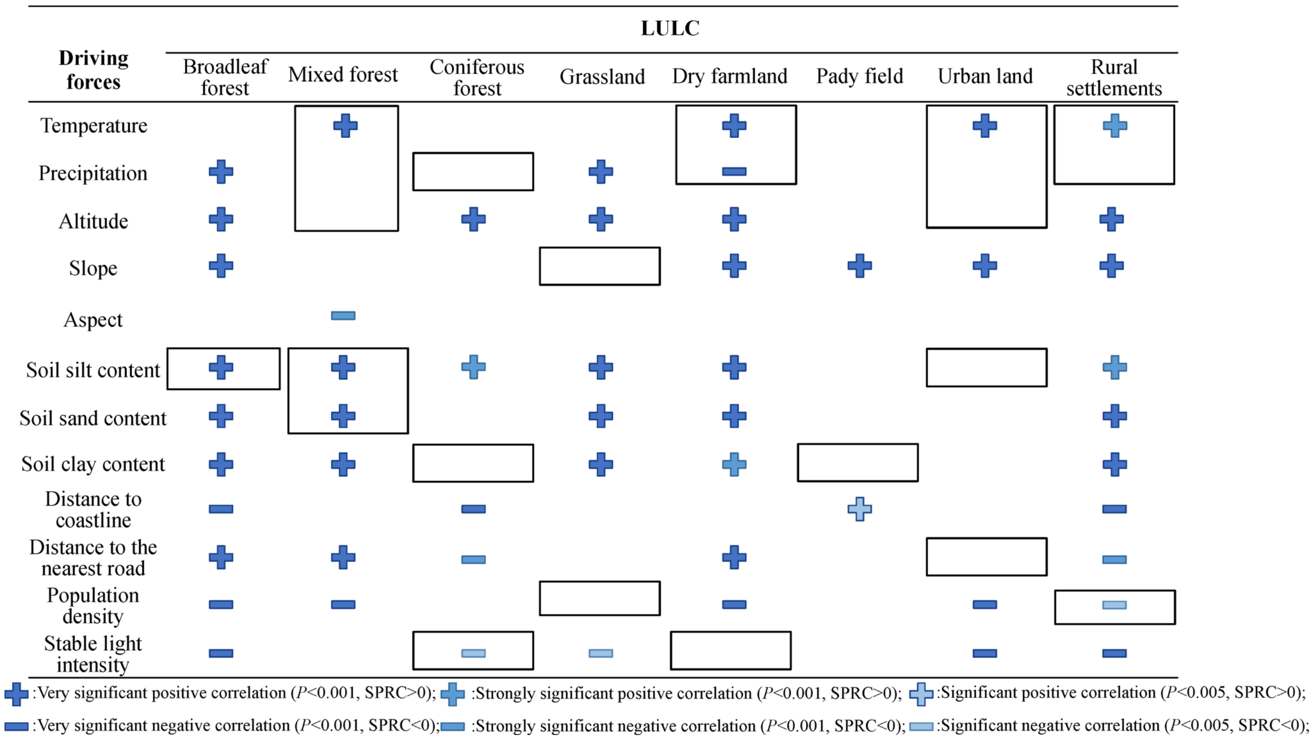

Fig. 5 The driving forces of the spatial pattern of NPP in the TATR in 2016.

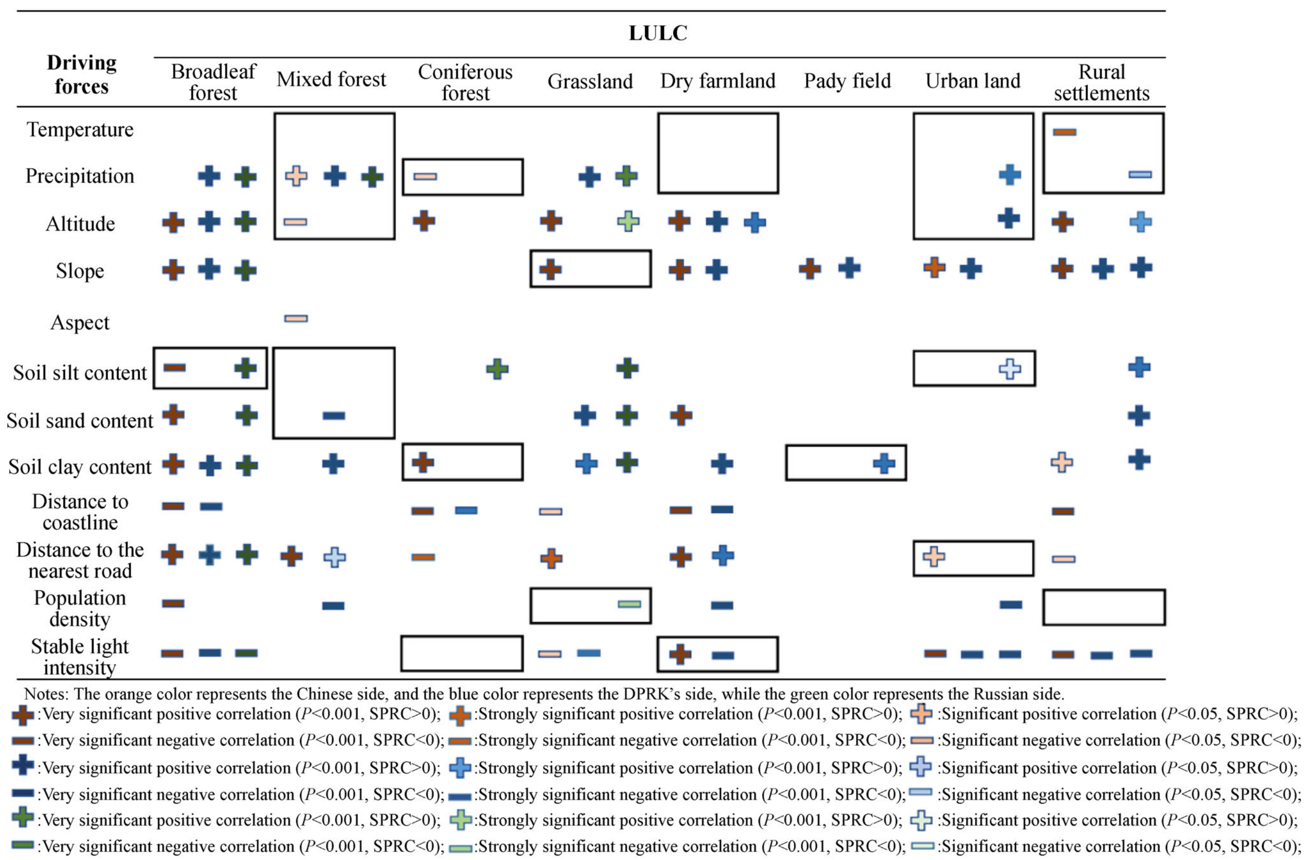

Fig. 6 The driving forces of the spatial pattern of NPP in the three sub-regions in 2016.

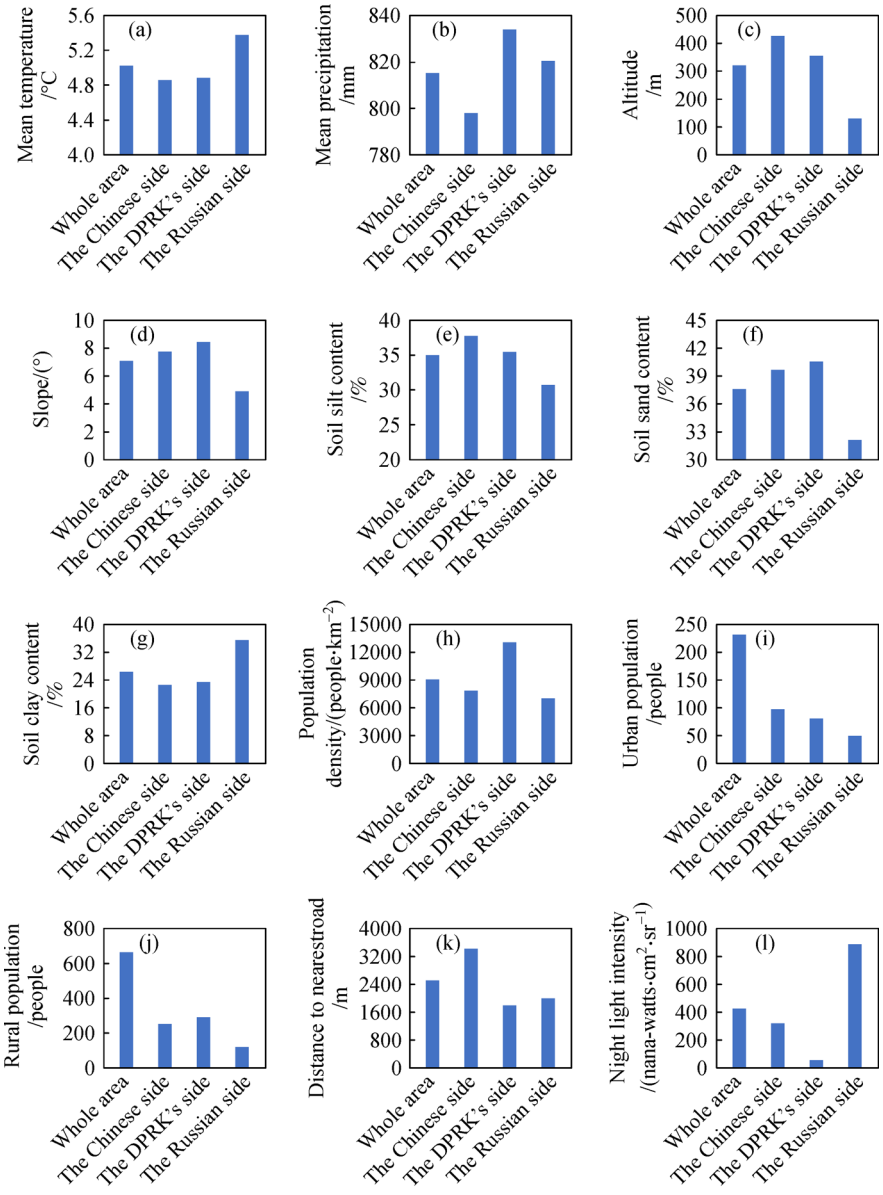

Fig. 7 The causes for the scaling effect of the driving forces of the spatial patterns of NPP in the TATR. (a) Mean temperature; (b) mean precipitation; (c) altitude; (d) slope; (e) soil silt content; (f) soil sand content; (g) soil clay content; (h) population density; (i) urban population; (j) rural population; (k) distance to the nearest road; (l) night light intensity.

in 1988, the amended "Land Management Law of the People's Republic of China" in 1998, the "Implementation program for the Northeast, Inner Mongolia and other key state-owned forest natural resources protection project" in 2000, "The Overall plan for land utilization of Yanbian Korean Autonomous Prefecture from 1997–2010" in 2005, "Measures For the Administration of Urban Greening of Yanbian Korean Autonomous Prefecture" in 2005, and "a new round for the overall program of Grain for Green" in 2014. Meanwhile, the DPRK published "Land and Environmental Conservation Management Law" in 1998 and "Environmental Protection Law" in 1999. Russia launched the "Natural Resources Protection law" in 1993, "Land Code of the Russian federation" in 2001, "Agricultural land circulation law of the Russian federation" in 2003, and "Forest code of the Russian federation" in 2006. However, the results still showed a declining tendency in the NPP of specific LULC on the Chinese side, DPRK side and Russian side after implementation of these policies and regulations (Nam, 2003; Kang et al., 2017).

Recently, the dramatic increase in population and increasing urbanization on the Chinese side, the fast development of tourism on the Russian side, and the continuous cropland reclamation in response to food

shortages on the DPRK side have led to the loss of cropland and woodland, which in turn caused the decrease of NPP (Quan, 2013). In addition, the cooperation among China, the DPRK, and Russia was insufficient and ineffective which did not conserve the NPP and improve the environmental sustainability in the TATR. For example, the "Measures for the Administration of Urban Greening of Yanbian Korean Autonomous Prefecture" was implemented on the Chinese side aimed to improve the NPP of urban land and the living environment of residents. However, there was no such policy applied in the DPRK and Russia. Therefore, we suggest that China, DPRK, and Russia should strengthen their cooperation and conduct effective measures to coordinate the conflicts between environmental protection and socioeconomic development with the goal of improving regional NPP and promoting environmental sustainability in the TATR.

5.4 Future perspectives

This study has certain limitations. First, due to the lack of field survey data, the maximum light energy efficiency in the CASA model was not localized, which means the accuracy of NPP can still be improved. Second, only the LULC data in 2016 was used in this study, and the spatial dynamics of NPP over a long period was not quantified. Finally, some problems originating from the mixed pixels in remote sensing data were not effectively resolved due to the availability of data. However, these limitations do not fundamentally affect the results above. We analyzed the spatial patterns of NPP and its driving forces in the TATR in 2016 on multiple scales. The outcome of this study will play an important role in understanding the driving mechanism of NPP and analyzing the ecological processes in the region.

In the future, the key parameters in the CASA model will be localized to improve the accuracy of NPP (Zhu et al., 2006). More remote sensing data will be used to analyze the spatiotemporal dynamics of NPP in this region (Chen et al., 2017). Finally, attempts will be made to resolve the mixed pixel problems in remote sensing data to quantify the spatial patterns of NPP more accurately and effectively.

6 Conclusions

In 2016, the total amount of NPP in the TATR was approximately 14.53 TgC. On the Chinese side, the total amount of NPP was about 6.23 TgC, accounting for 42.88% of the total amount across the whole region. For different LULC types, the total amount of NPP of broadleaf forest was the largest, i.e., 11.22 TgC. The mean NPP in summer was the highest, followed by spring and autumn, and the mean NPP in winter was the lowest. The mean value of NPP was approximately 603.21 $gC/(m^2 \cdot yr)$ in the entire region. On the three sides, the average NPP on the Chinese side was the largest, followed by the Russian side and the DPRK side.

In 2016, the spatial pattern of NPP in the TATR was mainly influenced by climate, topography, soil texture, and human activities. There were obvious differences for these driving forces in China, the DPRK, and Russia. The main driving forces of the spatial pattern of NPP on the Chinese side were distance to the coastline, slope, and nighttime light intensity, and the standard partial regression coefficients were -0.22, 0.32, and -0.38, respectively. The main driving forces on the DPRK side were clay content, distance to the coastline, and slope, while the coefficients were 0.27, 0.32, and 0.45, respectively. Meanwhile, soil clay content, altitude, and nighttime light intensity were the three major driving forces of the spatial pattern of NPP on the Russian side with the coefficients of 0.53, 0.12, and -0.5. In addition, the driving forces of the spatial pattern of NPP had an obvious scaling effect, which was mainly caused by the spatial heterogeneity of climate, topography, soil texture, and human activities. Therefore, we suggest that China, the DPRK, and Russia should collaborate to implement rational and efficient strategies to protect the natural environment to maintain and improve NPP, which will in turn to improve the sustainable development for the TATR.

Acknowledgements We also want to express our respects and gratitude to the anonymous reviewers and editors for their professional comments and suggestions. This work was supported by in part by the National Natural Science Foundation of China (Grant Nos. 41771094, 41501195, and 41801184).

Appendix

Table A1 Information on the Landsat data used in this study

Satellite	Sensor	Path/Row	Date
Landsat 8	OLI	114/30	12 October 2016
		114/31	12 October 2016
		115/30	28 May 2016
		115/31	28 May 2016

Table A2 Values of maximum light use efficiency

LULC	Maximum light use efficiency	Source
Broadleaf forest	0.838	Zhu et al. (2006)
Mixed forest	0.475	Zhu et al. (2006)
Coniferous forest	0.375	Zhu et al. (2006)
Grassland	0.608	Running et al. (2000)
Dry farmland	0.604	Running et al. (2000)
Paddy field	0.604	Running et al. (2000)
Marsh	0.542	Zhu et al. (2006)
Urban land	0.389	Running et al. (2000)
Rural settlements	0.389	Running et al. (2000)
River	0.389	Running et al. (2000)
Lake	0.389	Running et al. (2000)
Bare land	0.389	Running et al. (2000)

Table A3 The standardized partial regression coefficients of driving forces of spatial pattern of NPP in the entire region

Driving forces	LULC							
	Broadleaf forest	Mixed forest	Coniferous forest	Grassland	Dry farmland	Paddy field	Urban land	Rural settlements
Temperature	—	0.10***	—	—	0.36***	—	0.54***	0.14**
Precipitation	0.12***	—	—	0.21***	−0.29***	—	—	—
Altitude	0.15***	—	0.18***	0.12***	0.21***	—	—	0.24***
Slope	0.06***	—	—	—	0.26***	0.24***	0.29***	0.31***
Aspect	—	−0.10**	—	—		—	—	—
Soil silt content	0.17***	0.10***	0.10**	0.19***	0.16***	—	—	0.12**
Soil sand content	0.28***	0.14***	—	0.39***	0.24***	—	—	0.32***
Soil clay content	0.39***	0.11**	—	0.53***	0.09***	—	—	0.19***
Distance to coastline	−0.08***	—	−0.26***	—	−0.29***	0.11*	—	−0.30***
Distance to the nearest road	0.10***	0.14***	−0.09**	—	0.10***	—	—	−0.11**
Population	−0.03***	−0.36***	—	—	−0.09***	—	−0.23***	−0.08*
Light intensity	−0.09***	—	−0.06*	−0.05*	—	—	−0.45***	−0.18***

*represents $P < 0.05$, **represents $P < 0.01$, ***represents $P < 0.001$.

Table A4 The standardized partial regression coefficients of driving forces of spatial pattern of NPP on the Chinese side

Driving forces	LULC							
	Broadleaf forest	Mixed forest	Coniferous forest	Grassland	Dry farmland	Paddy field	Urban land	Rural settlements
Temperature	—	—	—	—	—	—	—	−0.22**
Precipitation	—	0.12*	−0.12*	—	—	—	—	—
Altitude	0.14***	−0.15*	0.22***	0.31***	0.18***	—	—	0.39***
Slope	0.05***	—	—	0.21***	0.32***	0.36***	0.20**	0.30***
Aspect	—	−0.12*	—	—	—	—	—	—
Soil silt content	−0.08***	—	—	—	—	—	—	—
Soil sand content	0.17***	—	—	—	0.21***	—	—	—
Soil clay content	0.05***	—	0.16***	—	—	—	—	0.14*
Distance to coastline	−0.22***	—	−0.25***	−0.14*	−0.24***	—	—	−0.34***

(*Continued*)

Driving forces	LULC							
	Broadleaf forest	Mixed forest	Coniferous forest	Grassland	Dry farmland	Paddy field	Urban land	Rural settlements
Distance to the nearest road	0.09***	0.22***	−0.13**	0.19**	0.15***	—	0.16*	−0.14*
Population	−0.07***	—	—	—	—	—	—	—
Light intensity	−0.14***	—	—	−0.13*	−0.11***	—	−0.38***	−0.19***

*represents $P < 0.05$, **represents $P < 0.01$, ***represents $P < 0.001$.

Table A5 The standardized partial regression coefficients of driving forces of spatial pattern of NPP on the DPRK's side

Driving forces	LULC							
	Broadleaf forest	Mixed forest	Coniferous forest	Grassland	Dry farmland	Paddy field	Urban land	Rural settlements
Temperature	—	—	—	—	—	—	—	—
Precipitation	0.19***	0.49***	—	0.22***	—	—	—	—
Altitude	0.17***	—	—	—	0.32***	—	—	—
Slope	0.08***	—	—	—	0.31***	0.30***	0.45***	0.43***
Aspect	—	—	—	—	—	—	—	—
Soil silt content	—	—	—	—	—	—	—	—
Soil sand content	—	−0.28***	—	0.34***	—	—	—	—
Soil clay content	0.27***	0.27***	—	0.24**	0.12***	—	—	—
Distance to coastline	−0.15***	—	−0.13**	—	−0.32***	—	—	—
Distance to the nearest road	0.06***	0.08*	—	—	0.07**	—	—	—
Population	—	−0.73***	—	—	−0.07***	—	—	—
Light intensity	−0.10***	—	—	−0.15**	−0.10***	—	−0.40***	−0.31***

*represents $P < 0.05$, **represents $P < 0.01$, ***represents $P < 0.001$.

Table A6 The standardized partial regression coefficients of driving forces of spatial pattern of NPP on the Russian side

Driving factors	LULC							
	Broadleaf forest	Mixed forest	Coniferous forest	Grassland	Dry farmland	Paddy field	Urban land	Rural settlements
Temperature	—	—	—	—	—	—	—	—
Precipitation	0.22***	0.43***	—	0.22***	—	—	0.17**	0.09*
Altitude	0.12***	—	—	0.07**	0.12**	—	0.27***	0.16**
Slope	0.04***	—	—	—	—	—	—	0.22***
Aspect	—	—	—	—	—	—	—	—
Soil silt content	0.26***	—	0.77**	0.22***	—	—	0.16*	0.17**
Soil sand content	0.44***	—	—	0.41***	—	—	—	0.39***
Soil clay content	0.53***	—	—	0.48***	—	0.78**	—	0.26***
Distance to coastline	0.08***	—	—	—	—	—	—	—
Distance to nearest road	0.06***	—	—	—	—	—	—	—
Population	—	—	—	−0.08**	—	—	−0.21***	—
Light intensity	−0.07***	—	—	—	—	—	−0.50***	−0.22***

*represents $P < 0.05$, **represents $P < 0.01$, ***represents $P < 0.001$.

References

Barnes M K, Morvan K B, Gavin H T, David J S, Claire E W, John B, Victor M-V, Timothy J S (2015). Temporal variability in total, micro- and nano- phytoplankton primary production at a coastal site in the Western English Channel. Prog Oceanogr, 137(B): 470–483

Chen C X, Xu Z X, Wang Z H, Liu C M (2014). Temporal-spatial change simulation and analysis of net primary productivity in Northeast China from 2001 to 2010. Resources Science, 36(11): 2401–2412

Chen C X, Xu Z X, Zhang S R, Wang Z H (2016). Response of NPP to climate change and human activities in the Heihe River basin. J Beijing Normal U N, 52(5): 571–579

Chen T, Huang Q H, Liu M, Li M C, Qu L, Deng S L, Chen D (2017). Decreasing net primary productivity in response to urbanization in Liaoning Province, China. Sustainability, 9(2): 162

Cramer W, Kicklighter D W, Bondeau A, Moore Iii B, Churkina G, Nemry B, Ruimy A, Schloss A L (1999). Comparing global models of terrestrial net primary productivity (NPP): overview and key results. Glob Change Biol, 5(S1): 46–55

Field C B, Randerson J T, Carolyn M (1995). Global net primary production: combining ecology and remote sensing. Remote Sens Environ, 51(1): 74–88

Gao H X (2000). Some method on treating the collinearity of independent variables in multiple linear regression. J Appl Stat Manageme, 19(5): 49–55

Garcia-Aguirre M C, Ortiz M A, Zamorano J J, Reyes Y (2007). Vegetation and landform relationships at Ajusco volcano Mexico, using a geographic information system (GIS). For Ecol Manage, 239 (1/3): 1–12

Grant J A, Quinn M S (2007). Factors influencing transboundary wildlife management in the North American Crown of the Continent. J Environ Plann Manage, 50(6): 765–782

Haberl H, Erb K H, Krausmann F, Gaube V, Bondeau A, Plutzar C, Gingrich S, Lucht W, Fischer-Kowalski M (2007). Quantifying and mapping the human appropriation of net primary production in earth's terrestrial ecosystems. Proc Natl Acad Sci USA, 104(31): 12942–12947

Hao R F, Yu D Y, Liu Y P, Liu Y, Qiao J M, Wang X, Du J S(2017). Impacts of changes in climate and landscape pattern on ecosystem services. Sci Total Environ, 579(19): 718–728

He C Y, Liu Z F, Xu M, Ma Q, Dou Y Y(2017). Urban expansion brought stress to food security in China: evidence from decreased cropland net primary productivity. Sci Total Environ, 576: 660–670

Huang S, Tan X, Xu W S, Wang Z, Chen H S (2015). Improved Beijing PM (10) Forecast Using Multi-model Sets and Multiple Linear Regression. J Environ Sci (China), 35(1): 56–64

Holben B N (1986). Characteristics of maximum-value composite images from temporal AVHRR data. Int J Remote Sens, 7(11): 1417–1434

IGBP (1998). The terrestrial carbon cycle: implications for Kyoto protocol. Science, 280(5368): 1393–1394

Imhoff M L, Bounoua L, DeFries R, Lawrence W T, Stutzer Z, Tucker C J, Ricketts T (2004). The consequences of urban land transformation on net primary productivity in the United States. Remote Sens Environ, 89(4): 434–443

Jian H Q (2010). Vegetation Ecology. Beijing: High Education Press

Jiang S F (2016). The study on land use/cover change and NPP remote sensing estimation of DPRK. Dissertation for Master's Degree. Yanji: Yanbian University

Kang C H, Zhang Y L, Wang Z F, Liu L S, Zhang H M, Jo Y W (2017). The driving force analysis of NDVI Dynamics in the trans-boundary Tumen River Basin between 2000 and 2015. Sustainability, 9(12): 2350

Li B, Liu Z F, Nan Y, Li S N, Yang Y M (2018). Comparative analysis of urban heat island intensities in Chinese, Russian, and DPRK Regions across the transnational urban agglomeration of the Tumen River in Northeast Asia. Sustainability, 10(8): 2637

Li Y L, Pan X Z, Wang C K, Liu Y, Zhao Q G (2014). Changes of vegetation net primary productivity and its driving factors from 2000 to 2011 in Guangxi, China. Acta Ecol Sin, 34(18): 5220–5228

Li Z, Pan J H (2018). Spatiotemporal changes in vegetation net primary productivity in the arid region of Northwest China, 2001 to 2012. Front Earth Sci, 12(1): 108–124

Liu Z F, Ding M H, He C Y, Li J W,Wu J G (2019). The impairment of environmental sustainability due to rapid urbanization in the dryland region of northern China. Landscape Urban Plan, 187: 165–180

Liu Z F, He C Y, Wu J G (2016). General spatiotemporal patterns of urbanization: an examination of 16 world cities. Sustainability, 8(1): 41

Los S O, Justice C O, Tucker C J (1994). A global 1Â° by 1Â° NDVI data set for climate studies derived from the GIMMS continental NDVI data. Int J Remote Sens, 15(17): 3493–3518

Mainuddin M, Kirby M (2009). Agricultural productivity in the lower Mekong Basin: trends and future prospects for food security. Food Secur, 1(1): 71–82

Mao D H, Wang Z M, Han J X, Ren C (2012a). Spatiotemporal patterns and driving factors of NPP in northeast in China from 1982–2012. Geographical Sci, 32(9): 1106–1111

Mao D H, Wang Z M, Luo L, Han J X (2012b). Dynamics of net primary productivity of permafrost in Northeast China from 1982 to 2009 and its response to global change. J Appl Ecol, 23(6): 1511–1519

Ma Q, Wu J G, He C Y, Hu G H (2018). Spatial scaling of urban impervious surfaces across evolving landscapes: from cities to urban regions. Landsc Ecol, 175: 50–61

Matsushita B, Tamura M (2002). Integrating remotely sensed data with an ecosystem model to estimate net primary productivity in East Asia. Remote Sens Environ, 81(1): 58–66

Nam S (2003). The Legal development of the environmental policy in the Democratic People's Republic of Korea. Acta Chir Iugosl, 31(1): 67–71

Nan Y, Ji Z, Fen H D, Zhang C C (2013). On eco-security evaluation in the Tumen River region based on RS&GIS. Acta Ecol Sin, 33(15): 4790–4798

Nan Y, Liu Z F, Dong Y H, Li X X, Ji Z (2010). The responses of vegetation cover to climate change in the Changbai Mountain Area from 2000 to 2008. Sciencia Geographyca Sinica, 30(6): 921–928

Potter C S, Randerson J T, Field C B, Matson P A, Vitousek P M, Mooney H A, Klooster S A (1993). Terrestrial ecosystem production— a process model based on global satellite and surface data. Global Biogeochem Cy, 7(4): 811–841

Prince S D, Goward S N (1995). Global primary production: a remote sensing approach. J Biogeogr, 22(4/5): 316–336

Quan Z N (2013). Food shortage problem of North Korea and its solution prospects. Cont Int Relat, 2013(01): 51–57

Ruimy A, Saugier B, Dedieu G (1994). Methodology for the estimation of terrestrial net primary production from remotely sensed data. J Geophys Res, 99(D3): 5263–5283

Running S W, Thornton P E, Nemani R, Glassy J M (2000). Global Terrestrial Gross and Net Primary Productivity from the Earth Observing System. New York: Springer Verlag

Sun Q L, Feng X F, Ge Y, Li B L (2015). Topographical effects of climate data and their impacts on the estimation of net primary productivity in complex terrain: a case study in Wuling mountainous area, China. Ecol Inform, 27(27): 44–54

Tao B, Li K R, Shao X M, Cao M G (2003). Simulation of spatial and temporal characteristics of net primary productivity in China. J Geogr Sci, 58(3): 372–380

Tao H, Nan Y, Liu Z F (2017). Spatiotemporal patterns of forest in the transnational area of Changbai Mountain from 1977 to 2015: a comparative analysis of the Chinese and DPRK sub-regions. Sustainability, 9(6): 1054

Wu J G (2004). The key research topics in landscape ecology. Acta Ecol Sin, 2004(09): 2074–2076

Yang Y M, Zhang D, Nan Y, Liu Z F, Zheng W (2019). Modeling urban expansion in the transnational area of Changbai Mountain: a scenario analysis based on the zoned Land Use Scenario Dynamics-urban model. Sustain Cities Soc, 50: 101622

You S B, Yan Y (2017). Stepwise regression analysis and its application. Stat Decis, 2017(14): 31–35

Zhan X, Liang X, Xu G, Zhou L (2013). Influence of plant root morphology and tissue composition on phenanthrene uptake: stepwise multiple linear regression analysis. Environ Pollut, 179(8): 294–300

Zhang D, Huang Q X, He C Y, Wu J G (2017). Impacts of urban expansion on ecosystem services in the Beijing-Tianjin-Hebei urban agglomeration, China: a scenario analysis based on the Shared Socioeconomic Pathways. Resources, Conserv Recycling, 125:115–130

Zhang D, Huang Q X, He C Y, Yin D, Liu Z W (2019). Planning urban landscape to maintain key ecosystem services in a rapidly urbanizing area: a scenario analysis in the Beijing-Tianjin-Hebei urban agglomeration, China. Ecol Indic, 96: 559–571

Zhang F, Zhou G S (2008). Spatial-temporal variations in net primary productivity along Northeast China Transect (NECT) from 1982–1999. J Plant Ecol, 32(4): 798–809

Zhang W T, Dong W (2007). Advanced Course in Statistical Analysis of SPSS. Beijing: Higher Education Press

Zhang Y S, Tang H M (2010). The opportunities and challenges of the regional development of Tumen River in China under the new situation. NE Asia Forum, 19(3): 11–16

Zhao L Q (2011). Spatial-temporal Patterns of the Vegetation Greenness Period and Net Primary Productivity and their Responses to Climate Change in the Middle and Lower Reaches of Yarlung Zangbu River. Dissertation for Master's Degree. Shanghai: East China Normal University

Zhu F, Liu Z M, Wang Z M, Song K S (2010). Temporal-spatial characteristics and factors influencing crop NPP across Northeastern China. Resources Sci, 32(11): 2079–2084

Zhu Q, Zhao J J, Zhu Z H, Zhang H Y, Zhang Z X, Guo X Y, Bi Y Z, Sun L (2017). Remotely sensed estimation of net primary productivity (NPP) and its spatial and temporal variations in the Greater Khingan Mountain Region, China. Sustainability, 9(7): 1213

Zhu W H, Miao C Y, Zhen X J, Cao G L, Wang F F (2014). Study on ecological safety evaluation and warning of wetlands in Tumen River watershed based on 3S technology. Acta Ecol Sin, 34(6): 1379–1390

Zhu W Q, Pan Y Z, He H, Yu D Y, Hu H (2006). Simulation of maximum light efficiency rate of typical vegetation in China. Chin Sci Bull, 51(4): 700–706

Zhu W Q, Pan Y Z, Zhu J S (2007). Estimation of net primary productivity of Chinese terrestrial vegetation based on remote sensing. Acta Phytoecol Sin, 31(3): 413–424

Zou J L (2015). The trade pattern and its economic contribution between China and the "Belt and Road" countries. Progr Geography, 34(5): 598–605